An Innovative BCS-Based Microwave Imaging Technique for Imaging Unknown Objects With Arbitrary Size and Shape

N. Alselmi, G. Oliveri, M. A. Hannan, M. Salucci, and A. Massa

Abstract

This work presents a numerical validation of an innovative two-dimensional (*2D*) microwave inverse scattering technique exploiting Bayesian Compressive Sensing (*BCS*) and a *dictionary* of wavelet-based expansion bases. The goal of the *dictionary-based BCS* is to provide faithful guesses of the dielectric distribution inside the imaged scenario even if the unknown objects inside it are not sparse in the standard pixel basis. The developed strategy is based on a two-level hierarchical application of the *BCS* algorithm. In the first step, several *sparsity-regularized* inversions are performed using the *dictionary* of candidate bases. In the second step, the retrieved vectors are compared and the sparsest reconstruction is selected. Some numerical results are shown, in order to verify the effectiveness of the developed microwave imaging technique. Moreover, some illustrative results are shown to compare its performance with respect to competitive state-of-the-art alternatives.

1 Numerical Results

1.1 Object Daub4 #0

Goal: To prove the effectiveness of the alphabet based approach using an "ad-hoc" scatterer for Daubechies wavelets.

Test Case Description

Object:

- $\varepsilon_{r,max} = 1.025$
- $\sigma = 0$ [S/m]
- Number of Daubechies coefficients: $Nc = 16$

Sources:

- Plane waves
- Amplitude: $A = 1$
- Frequency: 300 MHz ($\lambda = 1$m)
- Number of views: $V = 36$

Direct solver:

- Square domain divided in $\sqrt{D} \times \sqrt{D}$ cells
- $D = 4096$ (64×64) $(\frac{L_D}{\sqrt{D}} = \frac{\lambda}{16})$

Investigation domain:

- Square domain divided in $\sqrt{N} \times \sqrt{N}$ cells
- $N = 1024$ (32×32) $(\frac{L_D}{\sqrt{N}} = \frac{\lambda}{8})$
- $L_D = 4\lambda$

Measurement domain:

- Measurement points taken on a circle of radius $\rho = 4\lambda$
- $M = 36$

M-BCS parameters:

- $a = 1.0 \times 10^{-2}$
- $b = 1.0 \times 10^{-5}$

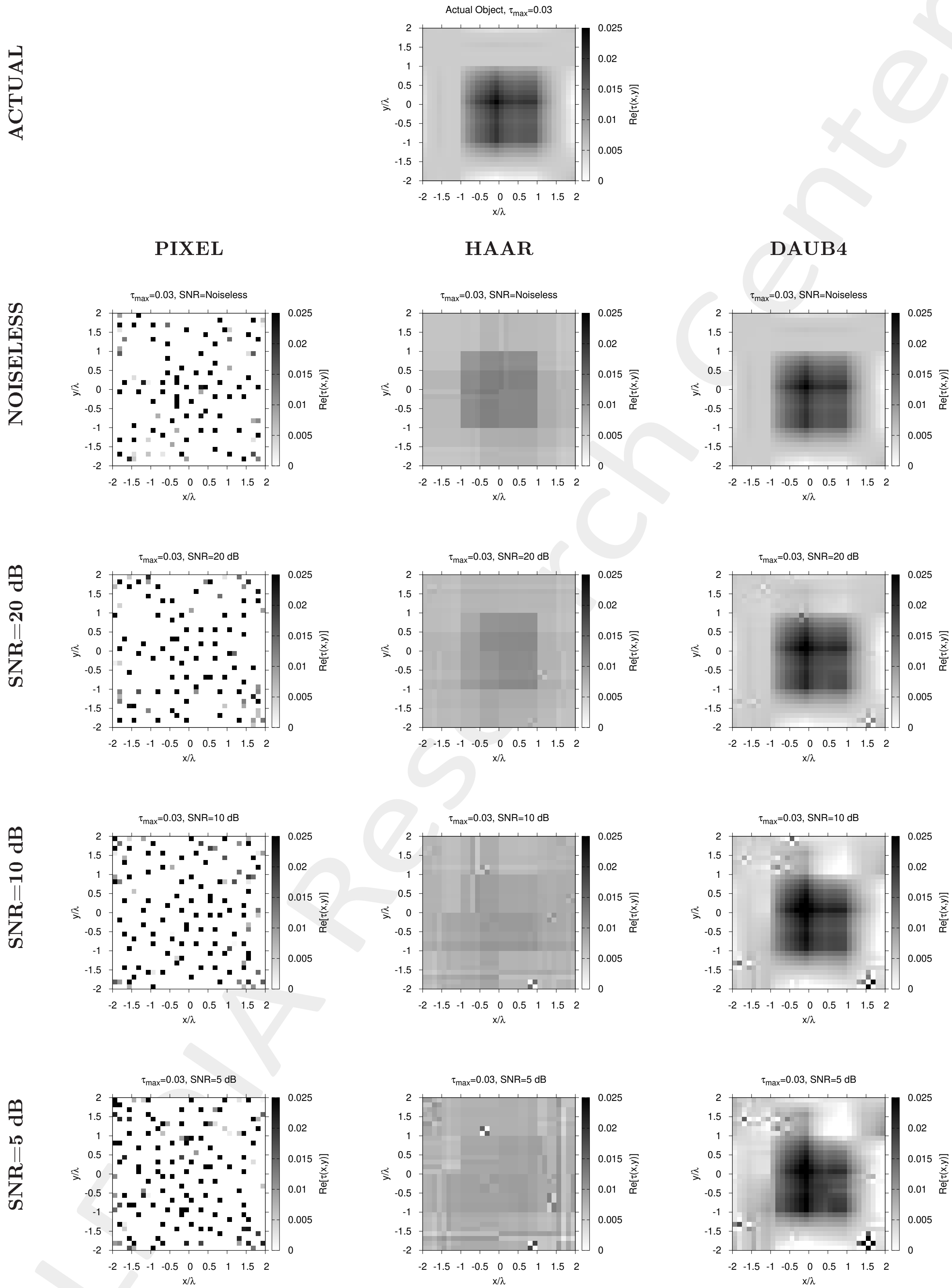

Figure 1: Actual and retrieved object (real part) considering different wavelet expansions.

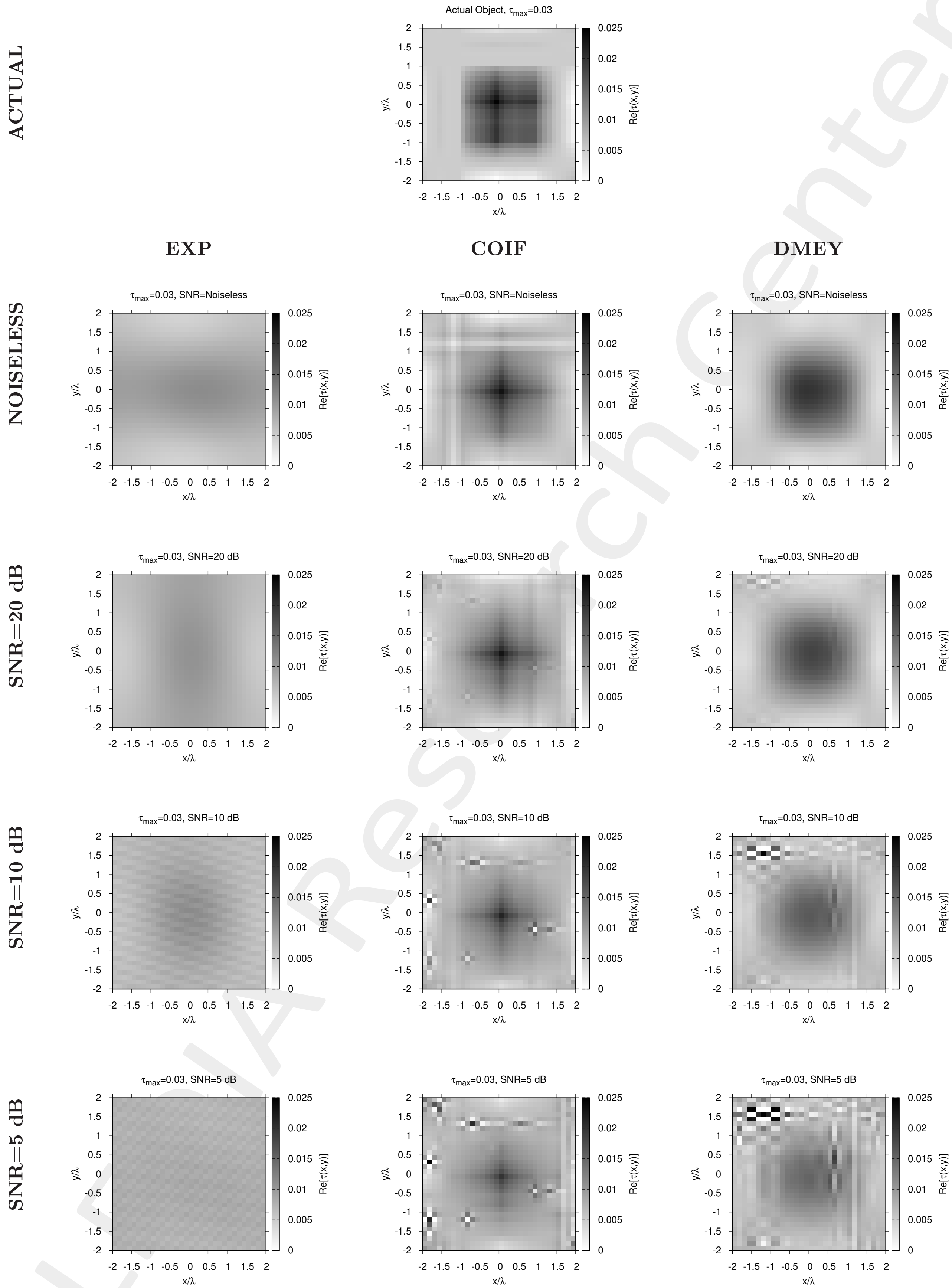

Figure 2: Actual and retrieved object (real part) considering different wavelet expansions.

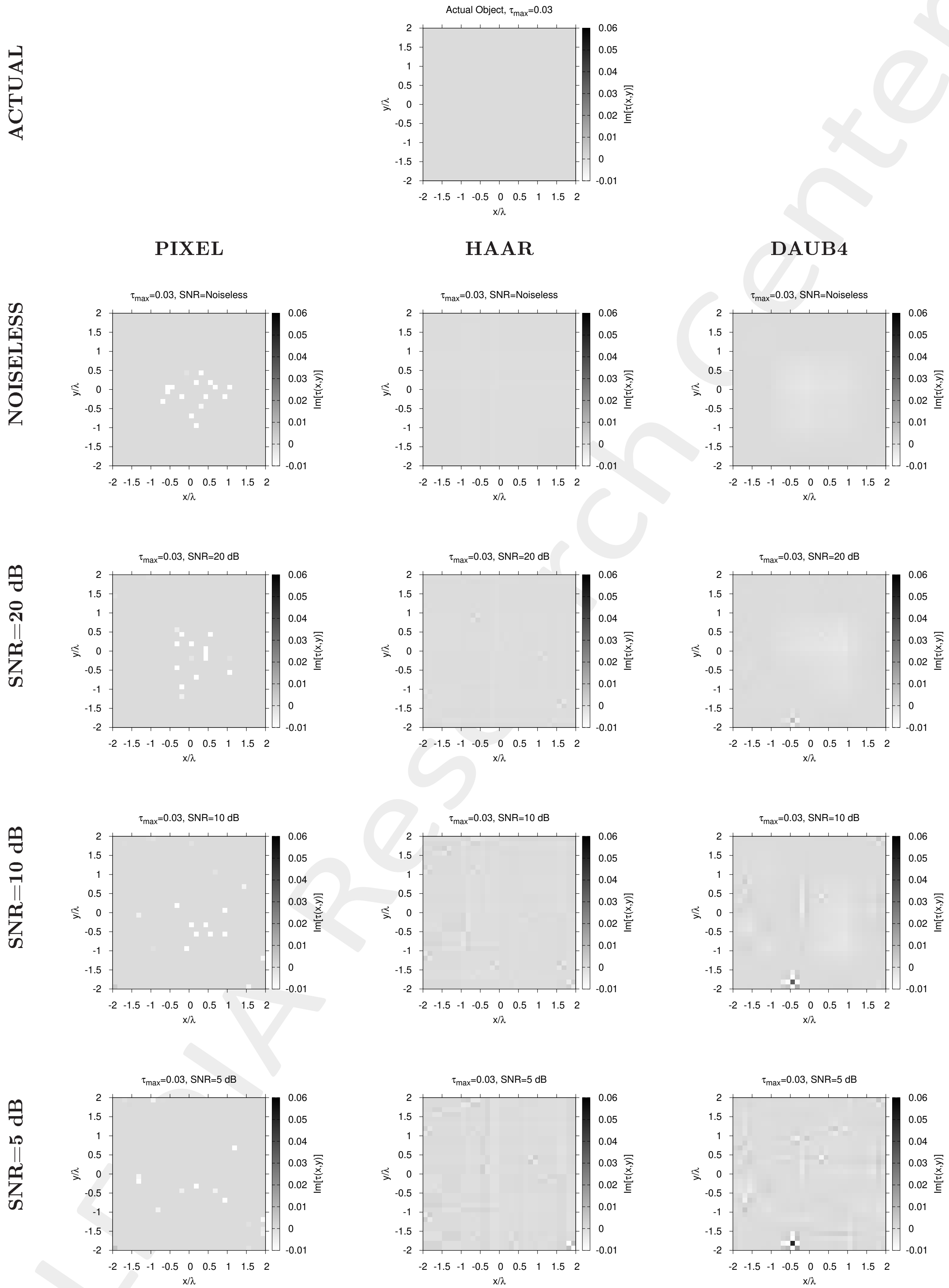

Figure 3: Actual and retrieved object (imaginary part) considering different wavelet expansions.

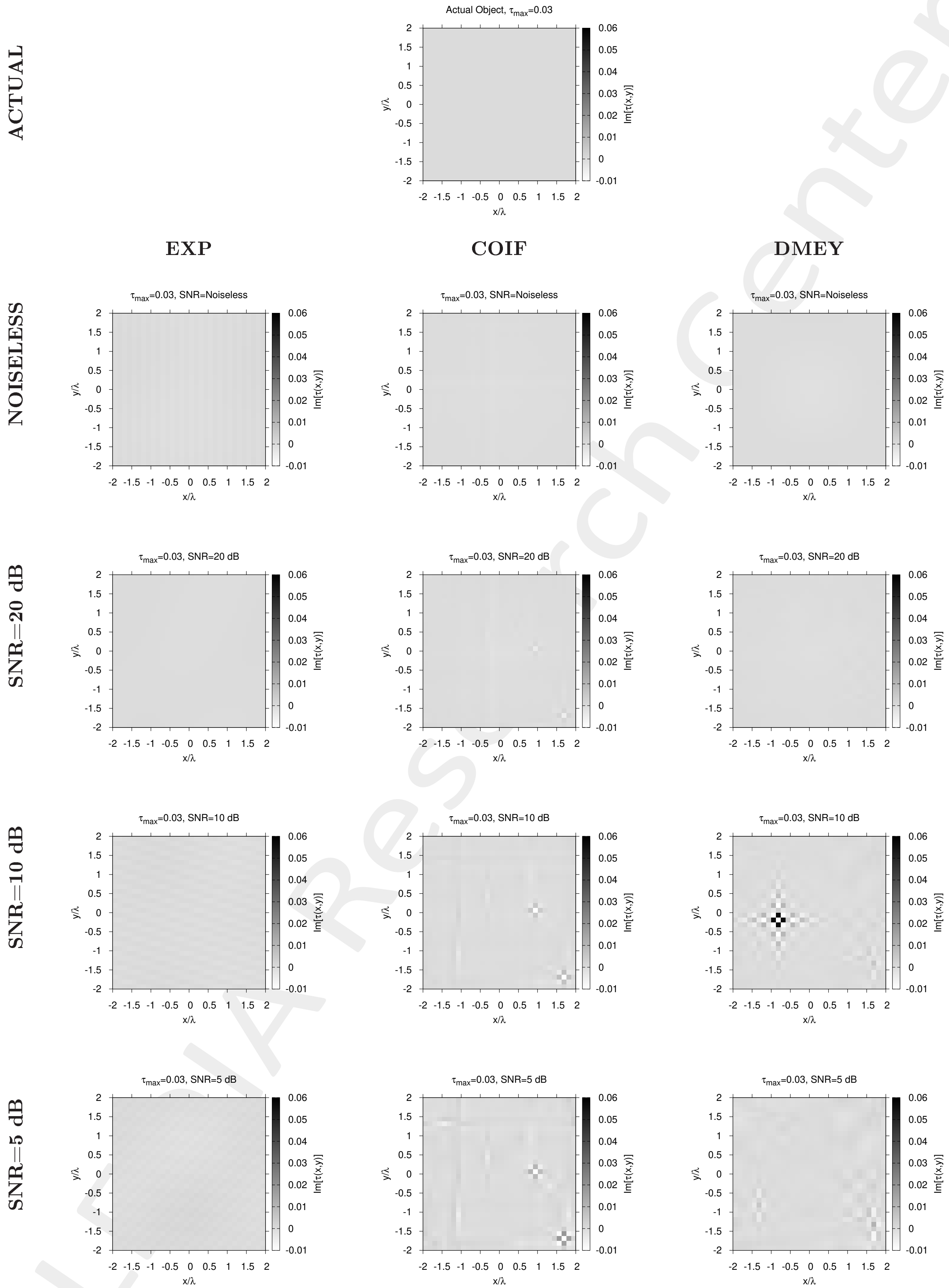

Figure 4: Actual and retrieved object (imaginary part) considering different wavelet expansions.

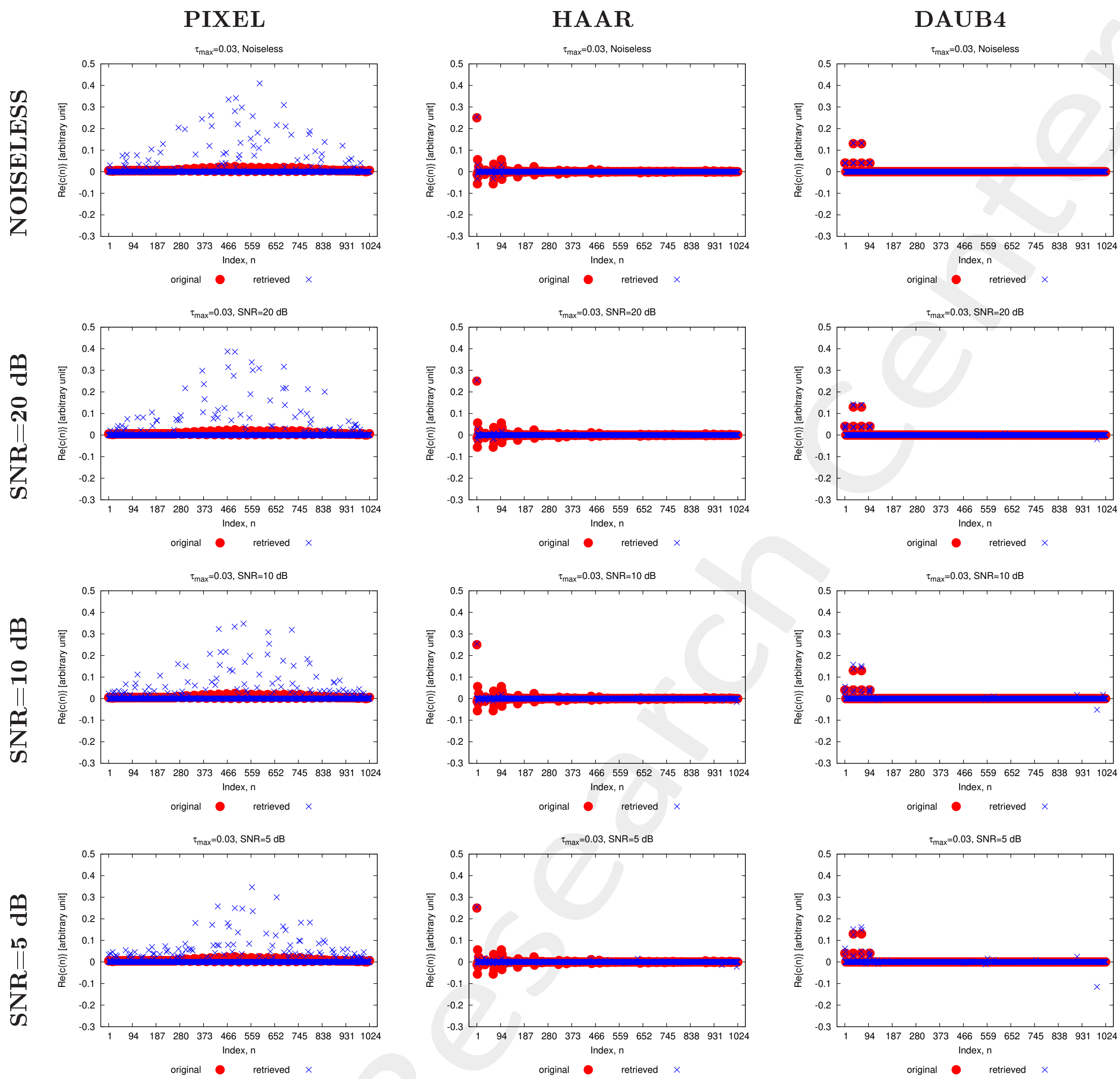

Figure 5: Real part of the actual and retrieved coefficients considering different wavelet expansions.

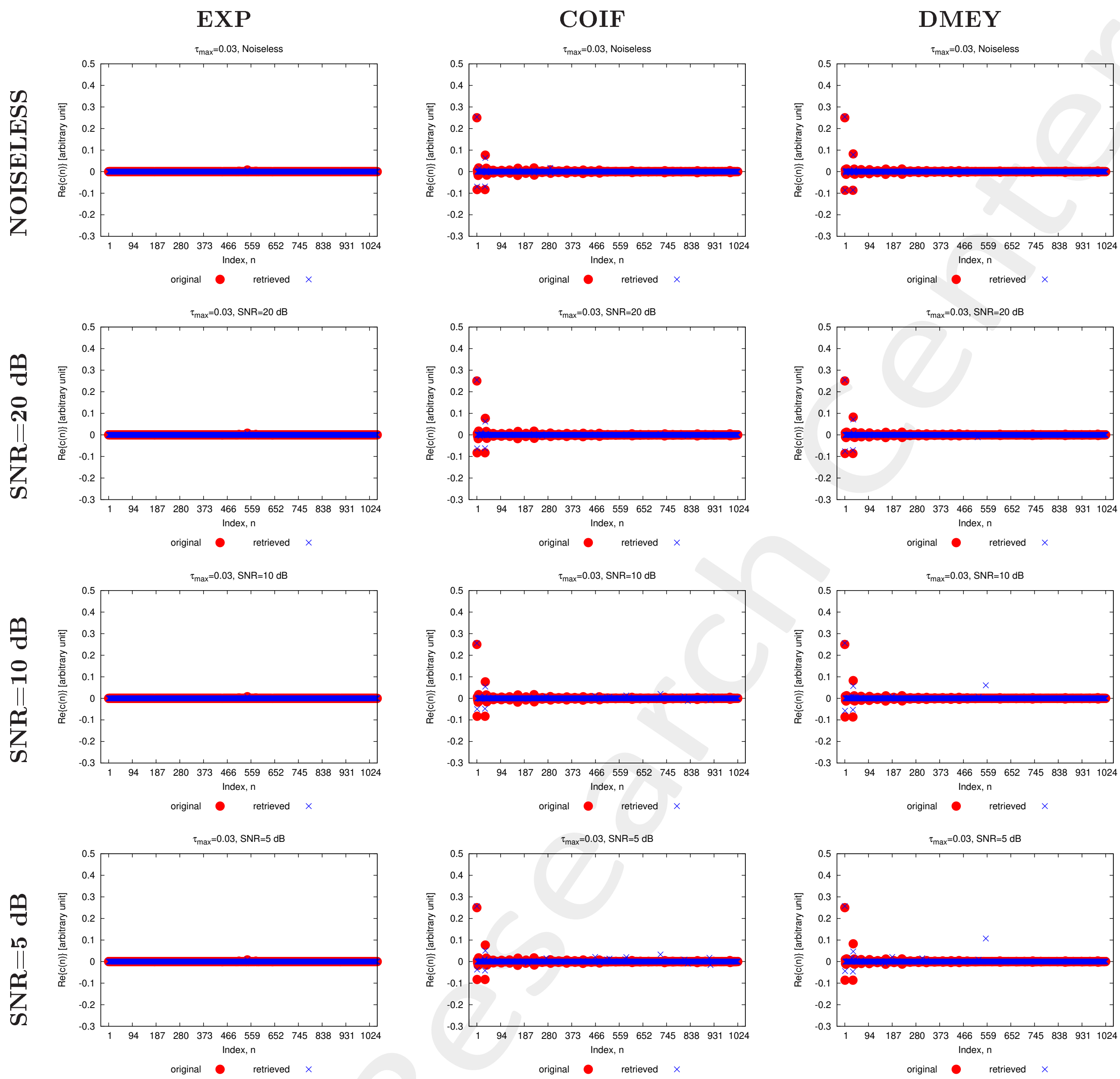

Figure 6: Real part of the actual and retrieved coefficients considering different wavelet expansions.

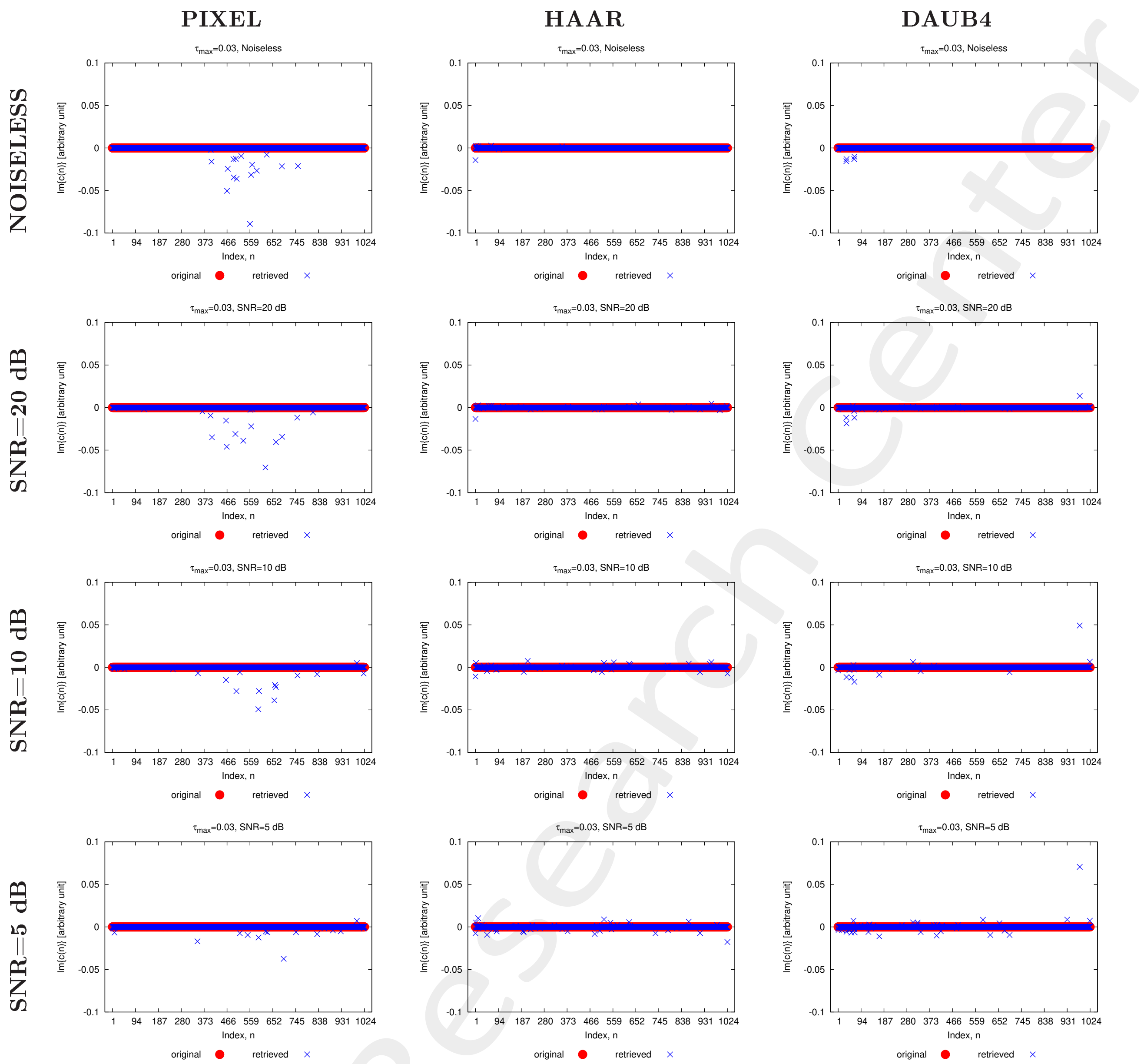

Figure 7: Imaginary part of the actual and retrieved coefficients considering different wavelet expansions.

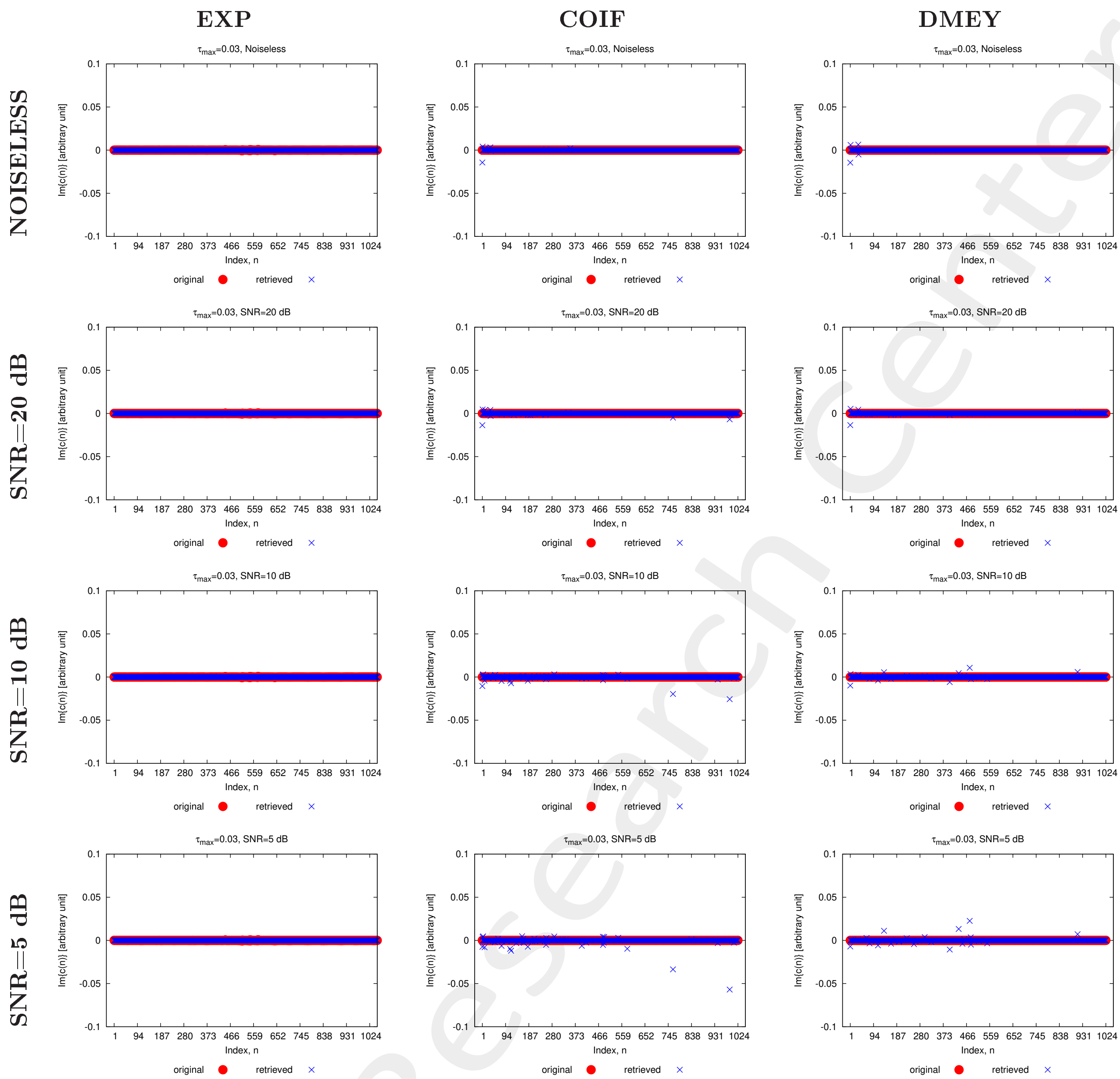

Figure 8: Imaginary part of the actual and retrieved coefficients considering different wavelet expansions.

Coefficients Analysis $T = 100\%$:

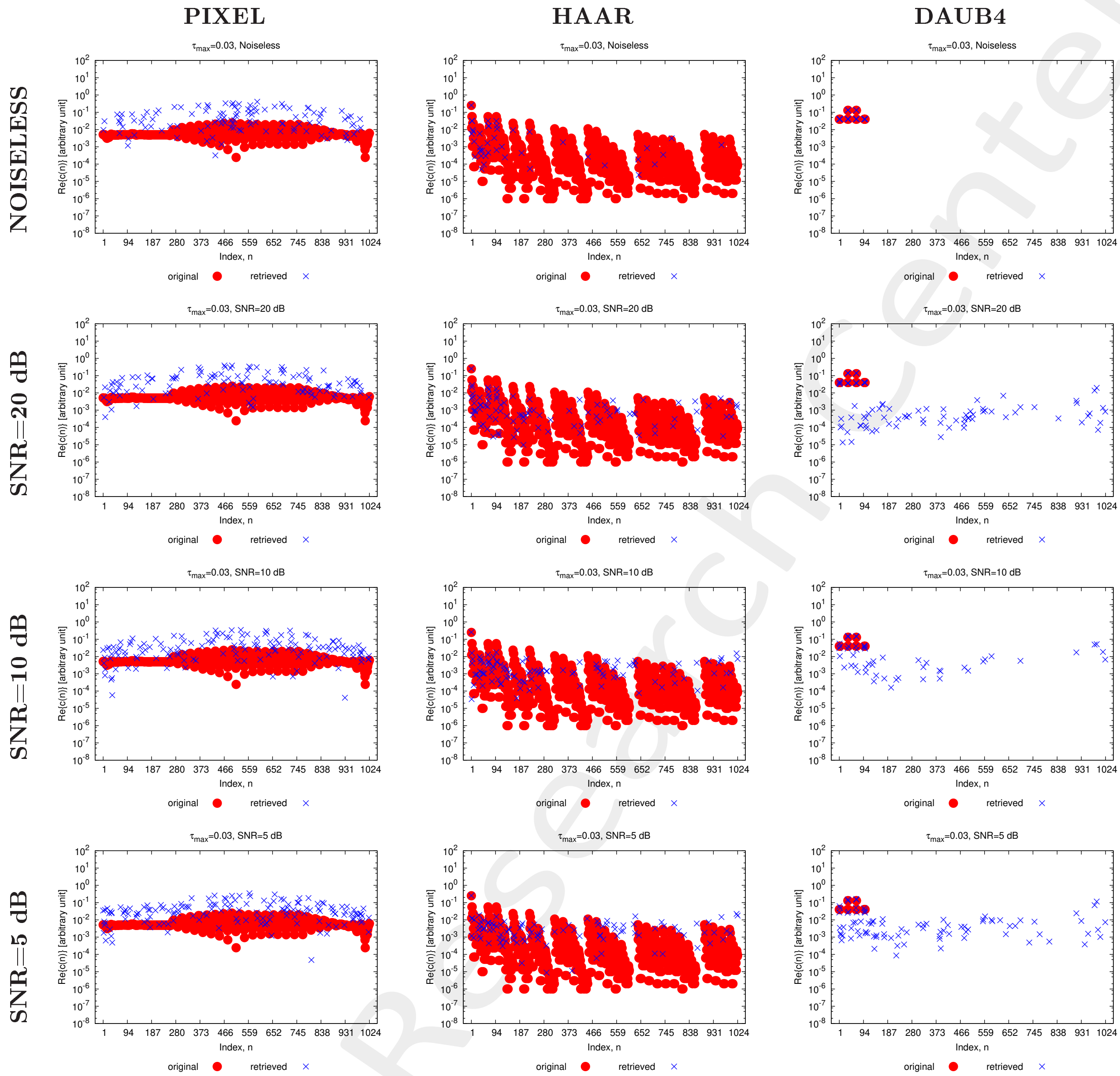

Figure 9: Imaginary part of the actual and retrieved coefficients considering different wavelet expansions.

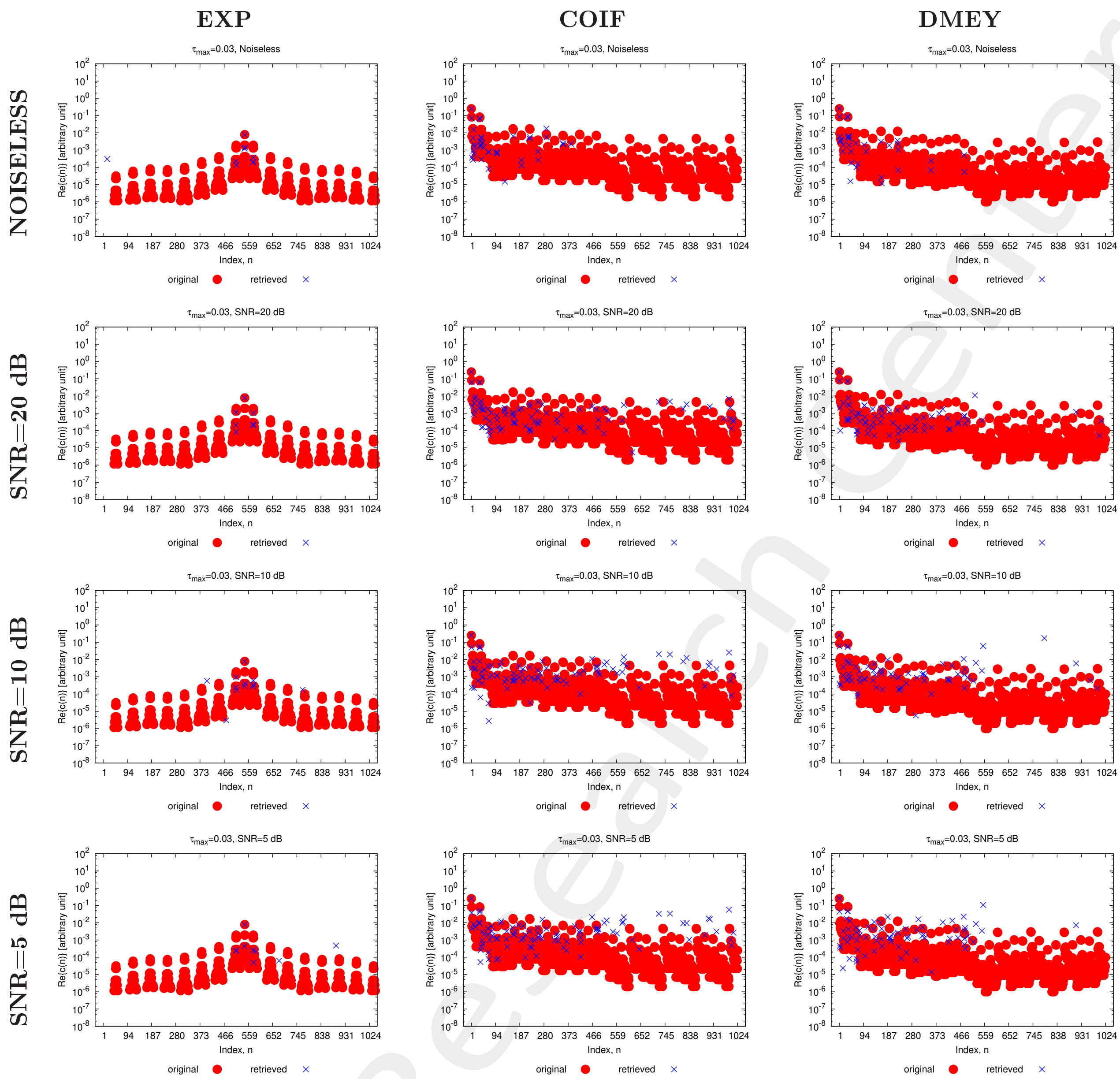

Figure 10: Imaginary part of the actual and retrieved coefficients considering different wavelet expansions.

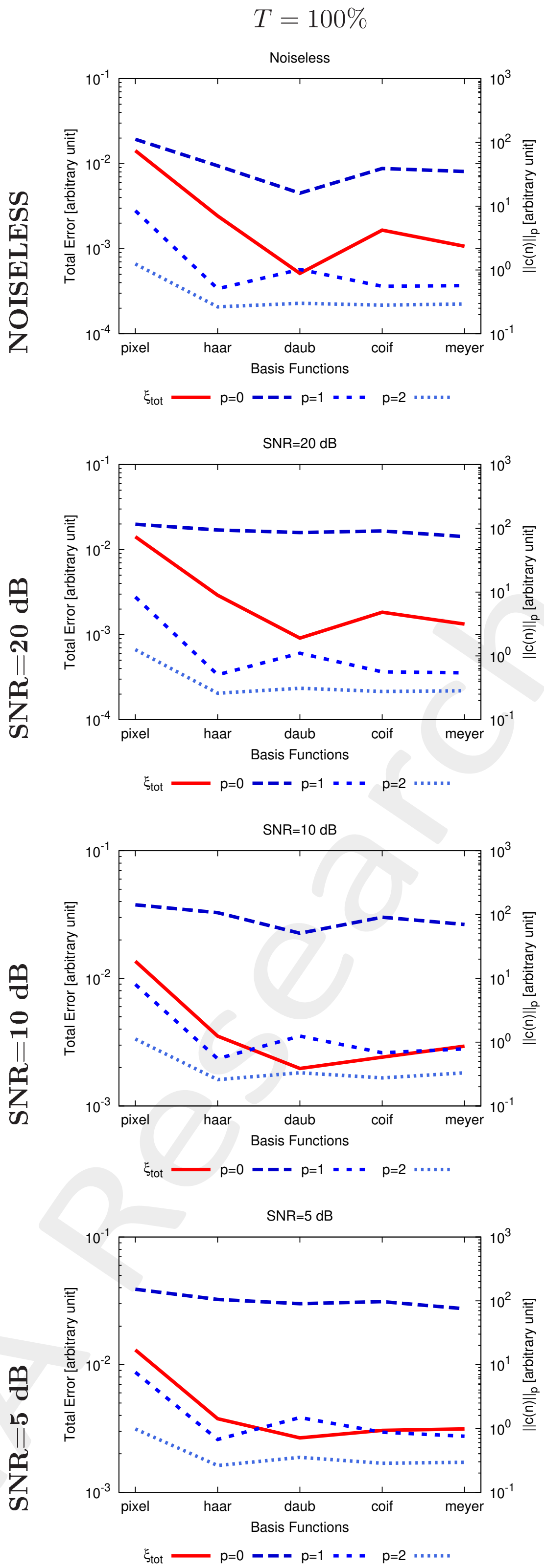

Figure 11: $[T = 100\%]$ - Comparison of ξ_{tot}, and L_0, L_1, L_2 Norms of the retrieved basis expansion coefficients, for each alphabet basis.

	$L_0 - norm$				
SNR [dB]	$Pixel$	$Haar$	$Daub4$	$Coiflet$	$DMeyer$
$Actual$	1024	888	16	1024	1024
$Noiseless$	112	43	**16**	39	35
20	116	94	86	91	**74**
10	142	107	**51**	91	70
5	152	105	90	97	**75**
	$L_1 - norm$				
SNR [dB]	$Pixel$	$Haar$	$Daub4$	$Coiflet$	$DMeyer$
$Actual$	8.00	1.48	1.00	1.25	1.02
$Noiseless$	8.50	0.51	1.02	0.56	0.57
20	8.41	0.51	1.10	0.56	0.54
10	8.03	0.55	1.25	0.68	0.79
5	7.60	0.67	1.48	0.87	0.75
	$L_2 - norm$				
SNR [dB]	$Pixel$	$Haar$	$Daub4$	$Coiflet$	$DMeyer$
$Actual$	0.29	0.29	0.29	0.29	0.29
$Noiseless$	1.24	0.26	0.30	0.38	0.29
20	1.26	0.26	0.31	0.27	0.28
10	1.12	0.26	0.33	0.28	0.33
5	0.97	0.26	0.35	0.28	0.29

Table 1: $[T = 100\%]$ - Number of the retrieved non-zero coefficients ($L_0 - norm$), $L_1 - norm$, and $L_2 - norm$ using different wavelet functions.

Thresholded Analysis:

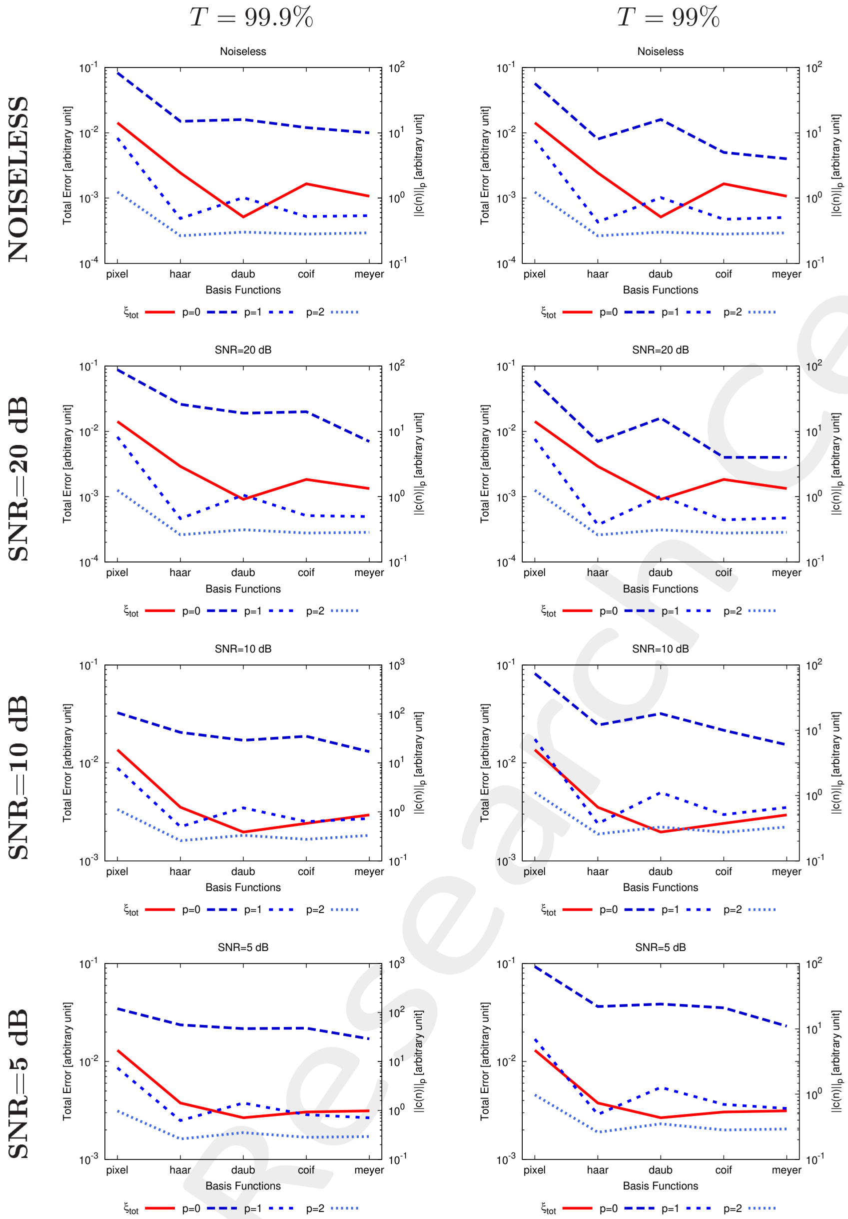

Figure 12: Comparison of ξ_{tot}, and L_0, L_1, L_2 Norms of the retrieved basis expansion coefficients, for each alphabet basis.

	$L_0 - norm$				
SNR [dB]	$Pixel$	$Haar$	$Daub4$	$Coiflet$	$DMeyer$
$Actual$	1024	888	16	1024	1024
$Noiseless$	83	15	16	12	10
20	88	26	19	20	7
10	106	42	29	35	17
5	120	56	47	48	29
	$L_1 - norm$				
SNR [dB]	$Pixel$	$Haar$	$Daub4$	$Coiflet$	$DMeyer$
$Actual$	8.00	1.48	1.00	1.25	1.02
$Noiseless$	8.31	0.49	1.02	0.52	0.54
20	8.23	0.46	1.06	0.51	0.50
10	7.86	0.50	1.21	0.63	0.73
5	7.44	0.62	1.42	0.82	0.71
	$L_2 - norm$				
SNR [dB]	$Pixel$	$Haar$	$Daub4$	$Coiflet$	$DMeyer$
$Actual$	0.29	0.29	0.29	0.29	0.29
$Noiseless$	1.24	0.26	0.30	0.28	0.29
20	1.26	0.26	0.31	0.28	0.28
10	1.12	0.26	0.33	0.28	0.33
5	0.98	0.26	0.35	0.28	0.29

Table 2: $[T = 99.9\%]$ - Number of the retrieved non-zero coefficients ($L_0 - norm$), $L_1 - norm$, and $L_2 - norm$ using different wavelet functions.

	$L_0 - norm$				
SNR [dB]	$Pixel$	$Haar$	$Daub4$	$Coiflet$	$DMeyer$
$Actual$	1024	888	16	1024	1024
$Noiseless$	57	8	16	5	4
20	59	7	16	4	4
10	74	12	18	10	6
5	90	22	24	21	11
	$L_1 - norm$				
SNR [dB]	$Pixel$	$Haar$	$Daub4$	$Coiflet$	$DMeyer$
$Actual$	8.00	1.48	1.00	1.25	1.02
$Noiseless$	7.74	0.43	1.02	0.47	0.51
20	7.62	0.37	1.02	0.44	0.47
10	7.3	0.37	1.11	0.51	0.66
5	6.96	0.49	1.27	0.70	0.60
	$L_2 - norm$				
SNR [dB]	$Pixel$	$Haar$	$Daub4$	$Coiflet$	$DMeyer$
$Actual$	0.29	0.29	0.29	0.29	0.29
$Noiseless$	1.24	0.26	0.30	0.28	0.29
20	1.25	0.26	0.31	0.28	0.28
10	1.11	0.26	0.33	0.27	0.33
5	0.97	0.26	0.35	0.28	0.29

Table 3: $[T = 99\%]$ - Number of the retrieved non-zero coefficients ($L_0 - norm$), $L_1 - norm$, and $L_2 - norm$ using different wavelet functions.

Resume:

	$T = 100\%$				
SNR [dB]	$Pixel$	$Haar$	$Daub4$	$Coiflet$	$DMeyer$
$Noiseless$	112	43	**16**	39	35
20	116	94	86	91	**74**
10	142	107	**51**	91	70
5	152	105	90	97	**75**
	$T = 99.9\%$				
SNR [dB]	$Pixel$	$Haar$	$Daub4$	$Coiflet$	$DMeyer$
$Noiseless$	83	15	16	12	**10**
20	88	26	19	20	**7**
10	106	42	29	35	**17**
5	120	56	47	48	**29**
	$T = 99\%$				
SNR [dB]	$Pixel$	$Haar$	$Daub4$	$Coiflet$	$DMeyer$
$Noiseless$	57	8	16	5	**4**
20	59	7	16	**4**	**4**
10	74	12	18	10	**6**
5	90	22	24	21	**11**

Table 4: $L_0 - norm$.

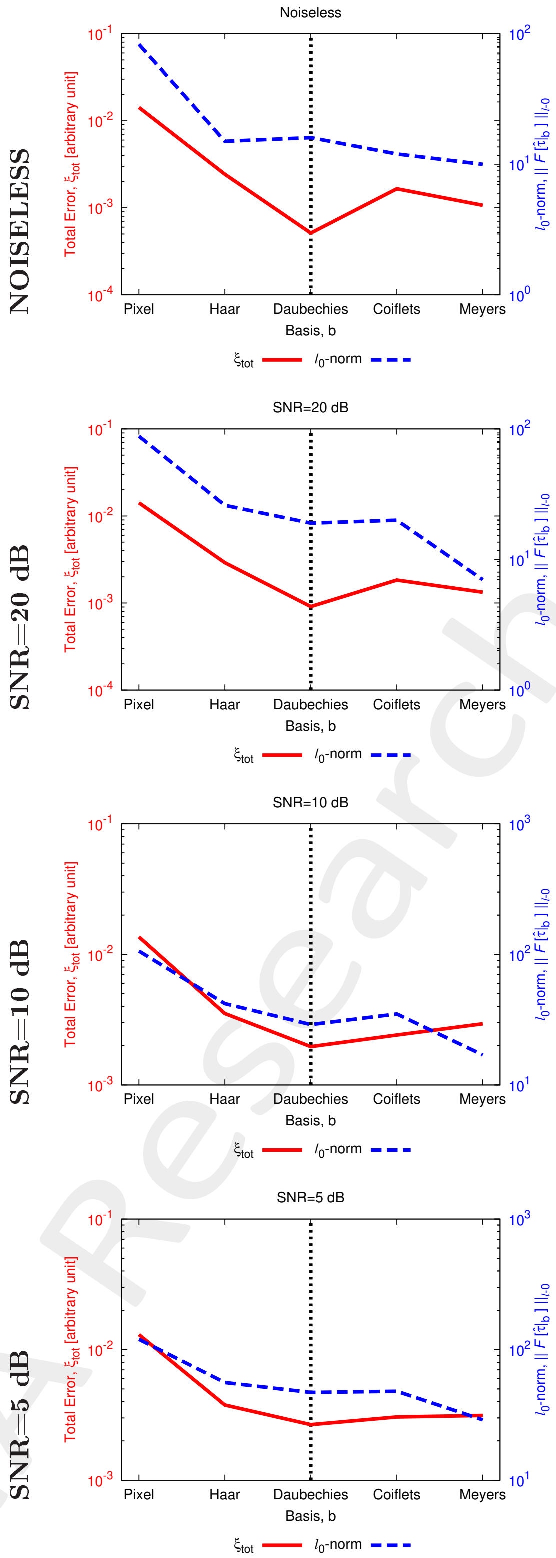

Figure 13: $L_0 - norm$ vs Total Error, considering $T = 99.9\%$.

Comparison SoA:

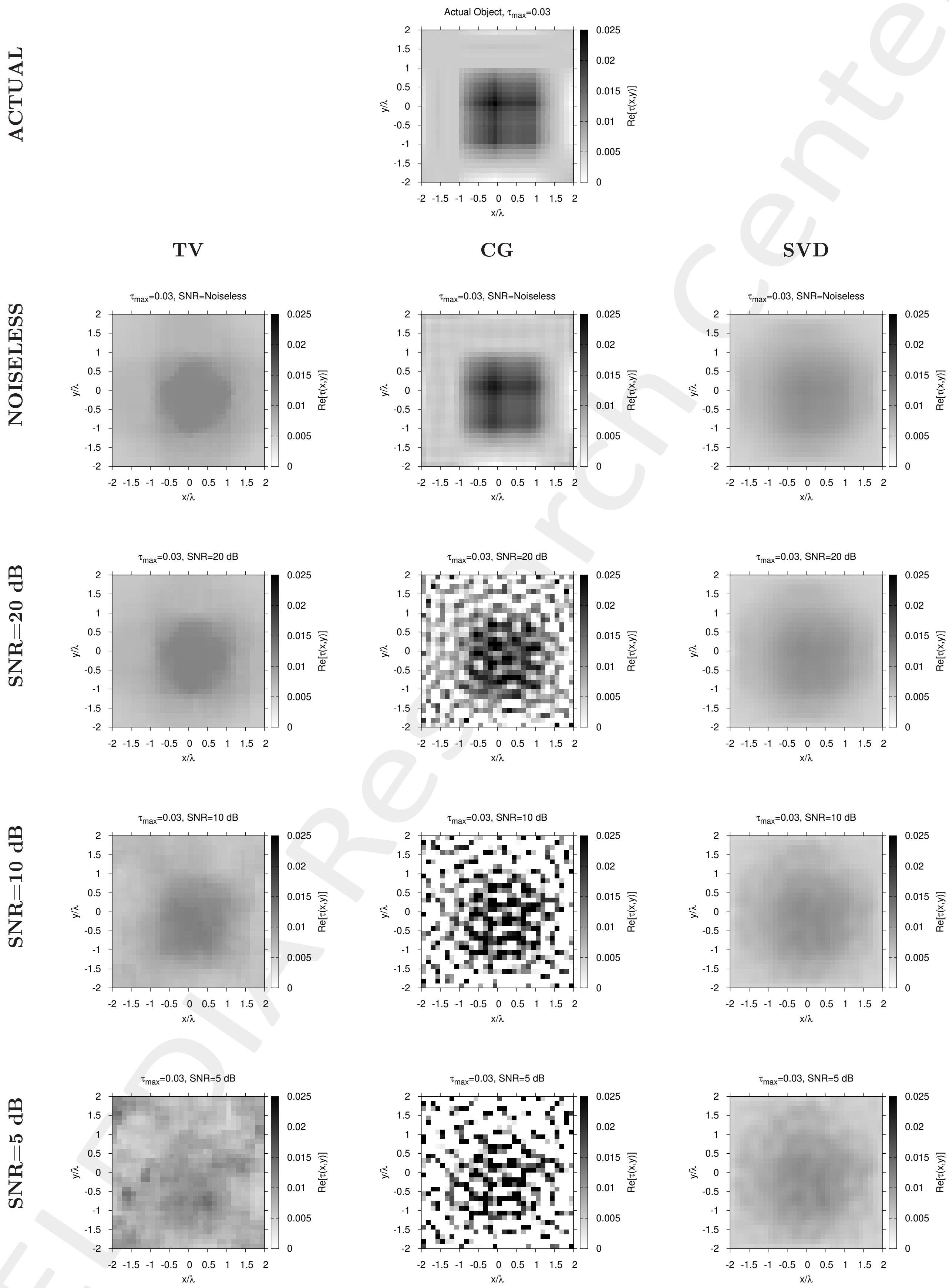

Figure 14: Actual and retrieved object considering different wavelet expansions.

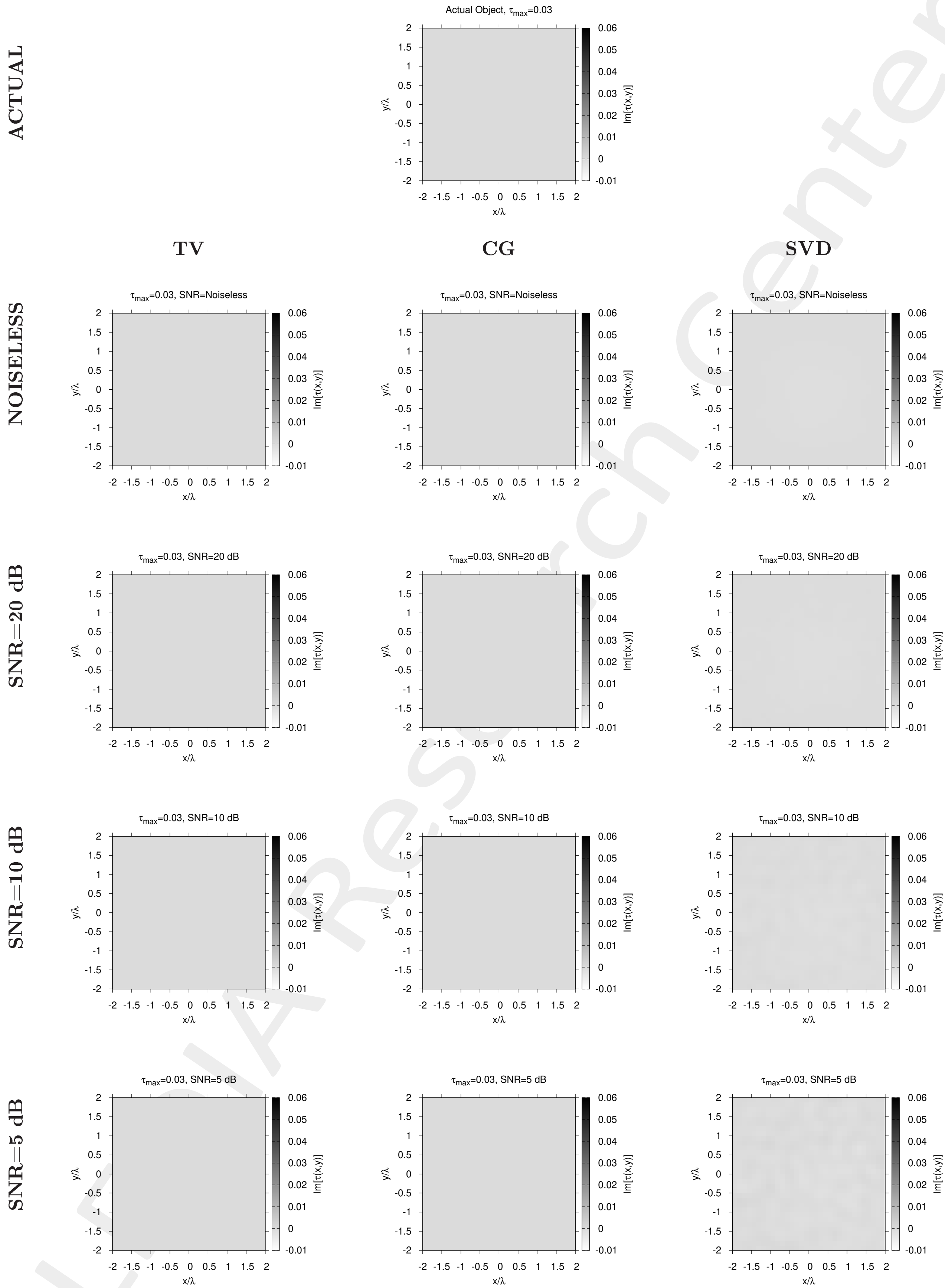

Figure 15: Actual and retrieved object considering different wavelet expansions.

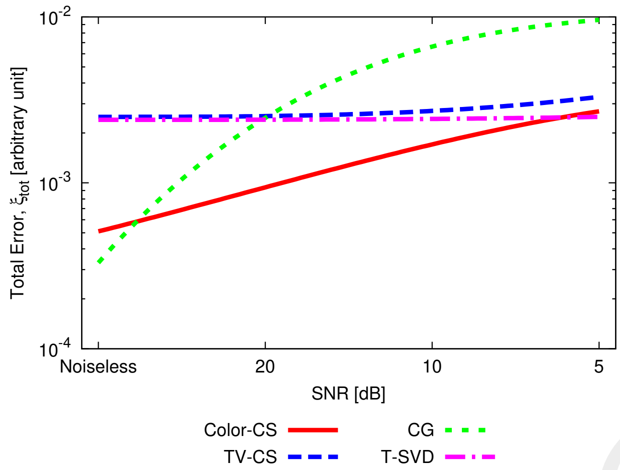

Figure 16: Comparison with SoA - Total Error vs SNR, considering $T = 99.9\%$.

SNR [dB]	**TV [s]**	**CG [s]**	**SVD [s]**	**ALPHABET [s]**
Noiseless	1.8×10^2	6.0×10^3	3.5×10^1	8.9×10^2
20	1.8×10^2	7.5×10^3	3.4×10^1	9.6×10^2
10	1.8×10^2	6.4×10^3	3.6×10^1	9.1×10^2
5	1.8×10^2	6.2×10^3	3.6×10^1	1.0×10^3

Table 5: Timings.

More information on the topics of this document can be found in the following list of references.

References

[1] A. Massa, P. Rocca, and G. Oliveri, “Compressive sensing in electromagnetics - A review,” *IEEE Antennas Propag. Mag.*, pp. 224-238, vol. 57, no. 1, Feb. 2015 (doi: 10.1109/MAP.2015.2397092).

[2] A. Massa and F. Texeira, “Guest-Editorial: Special Cluster on Compressive Sensing as Applied to Electromagnetics,” *IEEE Antennas Wirel. Propag. Lett.*, vol. 14, pp. 1022-1026, 2015 (doi: 10.1109/LAWP.2015.2425011).

[3] G. Oliveri, N. Anselmi, and A. Massa, “Compressive sensing imaging of non-sparse 2D scatterers by a total-variation approach within the Born approximation,” *IEEE Trans. Antennas Propag.*, vol. 62, no. 10, pp. 5157-5170, Oct. 2014 (doi: 10.1109/TAP.2014.2344673).

[4] L. Poli, G. Oliveri, and A. Massa, “Imaging sparse metallic cylinders through a Local Shape Function Bayesian Compressive Sensing approach,” *J. Opt. Soc. Am. A*, vol. 30, no. 6, pp. 1261-1272, 2013 (doi: 10.1364/JOSAA.30.001261).

[5] F. Viani, L. Poli, G. Oliveri, F. Robol, and A. Massa, “Sparse scatterers imaging through approximated multi-task compressive sensing strategies,” *Microwave Opt. Technol. Lett.*, vol. 55, no. 7, pp. 1553-1558, Jul. 2013 (doi: 10.1002/mop.27612).

[6] M. Salucci, G. Oliveri, and A. Massa, “GPR prospecting through an inverse scattering frequency-hopping multi-focusing approach,” *IEEE Trans. Geosci. Remote Sens.*, vol. 53, no. 12, pp. 6573-6592, Dec. 2015 (doi: 10.1109/TGRS.2015.2444391).

[7] M. Salucci, L. Poli, N. Anselmi and A. Massa, “Multifrequency particle swarm optimization for enhanced multiresolution GPR microwave imaging,” *IEEE Trans. Geosci. Remote Sens.*, vol. 55, no. 3, pp. 1305-1317, Mar. 2017 (doi: 10.1109/TGRS.2016.2622061).

[8] M. Salucci, L. Poli, and A. Massa, “Advanced multi-frequency GPR data processing for non-linear deterministic imaging,” *Signal Processing - Special Issue on ’Advanced Ground-Penetrating Radar Signal-Processing Techniques*,’ vol. 132, pp. 306-318, March 2017 (doi: 10.1016/j.sigpro.2016.06.019).

[9] L. Poli, G. Oliveri, P. Rocca, and A. Massa, “Bayesian compressive sensing approaches for the reconstruction of two-dimensional sparse scatterers under TE illumination,” *IEEE Trans. Geosci. Remote Sens.*, vol. 51, no. 5, pp. 2920-2936, May 2013 (doi: 10.1109/TGRS.2012.2218613).

[10] L. Poli, G. Oliveri, and A. Massa, “Microwave imaging within the first-order Born approximation by means of the contrast-field Bayesian compressive sensing,” *IEEE Trans. Antennas Propag.*, vol. 60, no. 6, pp. 2865-2879, Jun. 2012 (doi: 10.1109/TAP.2012.2194676).

[11] G. Oliveri, P. Rocca, and A. Massa, “A bayesian compressive sampling-based inversion for imaging sparse scatterers,” *IEEE Trans. Geosci. Remote Sens.*, vol. 49, no. 10, pp. 3993-4006, Oct. 2011 (doi: 10.1109/TGRS.2011.2128329).

[12] G. Oliveri, L. Poli, P. Rocca, and A. Massa, “Bayesian compressive optical imaging within the Rytov approximation,” *Optics Letters*, vol. 37, no. 10, pp. 1760-1762, 2012 (doi: 10.1364/OL.37.001760).

[13] L. Poli, G. Oliveri, F. Viani, and A. Massa, “MT-BCS-based microwave imaging approach through minimum-norm current expansion,” IEEE Trans. Antennas Propag., vol. 61, no. 9, pp. 4722-4732, Sep. 2013 (doi: 10.1109/TAP.2013.2265254).

[14] N. Anselmi, G. Oliveri, M. Salucci, and A. Massa, “Wavelet-based compressive imaging of sparse targets,” *IEEE Trans. Antennas Propag.*, vol. 63, no. 11, pp. 4889-4900, Nov. 2015 (doi: 10.1109/TAP.2015.2444423).

[15] N. Anselmi, G. Oliveri, M. A. Hannan, M. Salucci, and A. Massa, “Color compressive sensing imaging of arbitrary-shaped scatterers,” *IEEE Trans. Microw. Theory Techn.*, vol. 65, no. 6, pp. 1986-1999, Jun. 2017 (doi: 10.1109/TMTT.2016.2645570).

[16] F. Viani, G. Oliveri, and A. Massa, “Compressive sensing pattern matching techniques for synthesizing planar sparse arrays,” *IEEE Trans. Antennas Propag.*, vol. 61, no. 9, pp. 4577-4587, Sept. 2013 (doi: 10.1109/TAP.2013.2267195).

[17] G. Oliveri, M. Salucci, and A. Massa, “Synthesis of modular contiguously clustered linear arrays through a sparseness-regularized solver,” *IEEE Trans. Antennas Propag.*, vol. 64, no. 10, pp. 4277-4287, Oct. 2016 (doi: 10.1109/TAP.2016.2595623).

[18] P. Rocca, M. A. Hannan, M. Salucci, and A. Massa, “Single-snapshot DoA estimation in array antennas with mutual coupling through a multi-scaling BCS strategy,” *IEEE Trans. Antennas Propag.*, vol. 65, no. 6, pp. 3203-3213, Jun. 2017 (doi: 10.1109/TAP.2017.2684137).

[19] P. Rocca, M. Benedetti, M. Donelli, D. Franceschini, and A. Massa, “Evolutionary optimization as applied to inverse problems,” *Inverse Probl.*, vol. 25, pp. 1-41, Dec. 2009 (doi: 10.1088/0266-5611/25/12/123003).

[20] P. Rocca, G. Oliveri, and A. Massa, “Differential Evolution as applied to electromagnetics,” *IEEE Antennas Propag. Mag.*, vol. 53, no. 1, pp. 38-49, Feb. 2011 (doi: 10.1109/MAP.2011.5773566).